

Reliable and efficient numerical simulation of a model of tissue differentiation in a bone chamber¹

A. Gerisch², L. Geris³, H. Van Oosterwyck³, J. Vander Sloten³, R. Weiner²

Abstract

For the study of peri-implant tissue differentiation, a repeated sampling bone chamber has been developed. Mathematical models that describe tissue differentiation help to gain insight into the processes taking place in the chamber. We consider here the numerical solution of a taxis-diffusion-reaction partial differential equation model. The general approach is the method of lines and we pay special attention to transfer qualitative features of the solution to the numerical approximation. These features are the conservation of mass principle and the nonnegativity of concentration values. This is achieved by following the finite volume idea and by employing positivity preserving spatial discretisations, respectively. An instructive example is given. The time integration is performed with ROWMAP, a suitable implicit time integration method with time step size control. Altogether this yields a reliable and efficient numerical solution technique. A numerical simulation of the tissue differentiation process in the chamber is presented and discussed.

1 Introduction

Identifying and understanding the processes involved in bone growth and (re)modelling is an active research theme with profound clinical applications, *e.g.* for optimizing the treatment of bone fractures and the osseointegration of implants, alongside its importance in unravelling aspects of the development and growth of the human skeleton. The processes involved in embryonic skeletal development, in postnatal bone growth, and in fracture healing (in case of moderate fracture gap size and stability) are in many aspects very similar. In particular the aggregation of mesenchymal stem cells, their subsequent chondrification, *i.e.* the formation of cartilage, and finally ossification are shared

¹ This manuscript appears as Report on Numerical Mathematics No. 04-26, Martin-Luther-Universität Halle-Wittenberg, Germany, September 28, 2004, see <http://www.mathematik.uni-halle.de/reports/>. Submitted for publication.

² Martin-Luther-Universität Halle-Wittenberg, FB Mathematik und Informatik, Institut für Numerische Mathematik, 06099 Halle (Saale), Germany, gerisch@mathematik.uni-halle.de.

³ Division of Biomechanics and Engineering Design, Faculty of Engineering, Katholieke Universiteit Leuven, Celestijnenlaan 200A, Leuven B-3000, Belgium, liesbet.geris@mech.kuleuven.ac.be.

in all three cases [Vortkamp *et al.* 1998]. Out of the three examples, fracture healing provides the best opportunity to study the processes in an experimentally controllable environment. However, the reproducibility of animal experiments is still rather low since their outcome is often considerably site-specific and species-specific [Carter 1984, Bertram and Swartz 1991]. A repeated sampling bone chamber (Fig. 1) has been developed [Duyck *et al.* 2004] that enables the repetition of experiments at the same site in the same animal and hence overcomes the above restriction. Reliable repetition of experiments also allows for an improved validation of mathematical models and opens up the possibility of parameter estimation in the processes under study. Numerical simulation of the processes in the bone chamber in turn contributes to a better understanding of the experimentally observed phenomena and helps to gain insight into the mechanisms that are very hard to investigate experimentally [Geris *et al.* 2004].

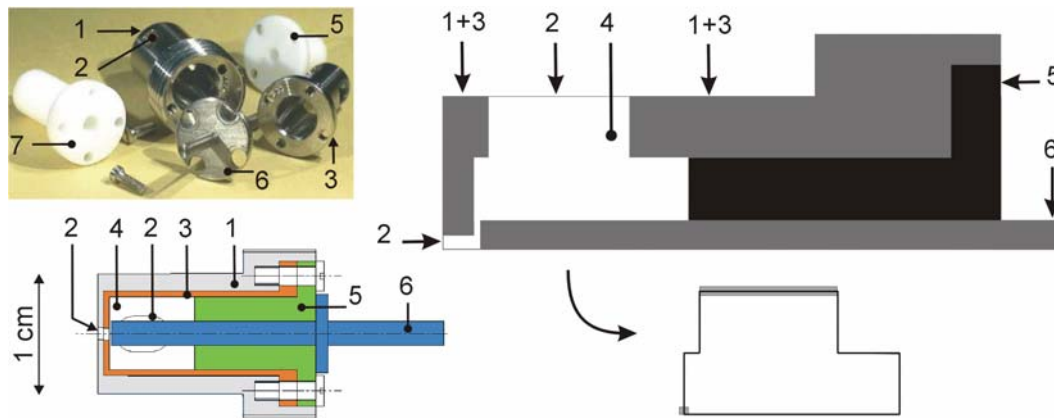


Fig. 1: Left: picture and composition-drawing of the bone chamber. After insertion of the outer bone chamber (1) in the rabbit's proximal tibia, there is a healing period of six weeks during which bone ingrowth is inhibited by a teflon inner chamber (7). After six weeks this inner chamber is removed and replaced with an inner chamber (3), a teflon bearing (5) and an implant (6). Tissue can grow through the perforations (2) into the free space (4) of the bone chamber. Right: axisymmetric model of the bone chamber (upper), and simplified FD/FV-model of the tissue (3) inside the chamber (lower).

Different mathematical models aim to describe the influence of different mechanical and biological parameters on bone tissue differentiation at different levels. The mechanoregulatory models developed by Prendergast *et al.* [1997] and Claes *et al.* [1999] describe the influence of mechanical loading on tissue differentiation on a continuum scale (macro level). In every element of the continuum finite element model, variables representing the local mechanical environment are calculated and based upon their values, the parameters of the mathematical models are adjusted. The biological model developed by Bailón-Plaza and van der Meulen [2001] also aims to simulate the tissue differentiation in fracture healing on a macro scale, taking only biological parameters into account.

In vitro studies show that in order to induce any cellular response by direct mechanical deformation of bone cells, deformations need to be one to two orders of magnitude larger than the bone tissue strains normally experienced by the

whole bone [You *et al.* 2001]. You and co-workers [2001] developed a model that links the loading on the whole bone to the loading that is sensed by individual cells. This way tissue differentiation can be linked to events happening at a cellular (micro) level.

One order of magnitude down (subcellular level), links have been established between integrin-mediated cell adhesion (which is central to cell survival, differentiation and motility) and biochemical and biophysical cues such as ligand spatial arrangement and matrix rigidity, which in turn are central to the governance of cell responses to the external environment [Koo *et al.* 2001]. Incorporation of these underlying processes in the mathematical models would result in a highly mechanistic model that describes bone tissue differentiation from the macro to the nano scale. The down-side of such a model is the very high number of unknown parameters and variables, of which most cannot be validated experimentally.

The study presented here focuses on the macro-level and looks into the effect of biological factors on bone tissue differentiation as described by the model of Bailón-Plaza and van der Meulen [2001]. In contrast to that work, which considers a ‘normal’ fracture, here, bone ingrowth into the bone chamber is considered. We present the model equations in Section 2.1, and our numerical approach to their solution in Section 2.2. In Section 2.3, we discuss the spatial discretisation of the linear advection equation, which is obtained as a very simplified version of the full model. Here we also make clear why we cannot be content with standard discretisations for the full model but need to use suitable schemes. Finally, in Section 3, we present some simulation results, compare with experimental observation, and give some concluding remarks.

2 Methods

2.1 Mathematical model

The mathematical model of tissue differentiation by Bailón-Plaza and van der Meulen [2001] is a partial differential equation (PDE) system of taxis-diffusion-reaction (TDR) type whose solution describes the evolution of seven quantities: mesenchymal (c_m), chondrocyte (c_c) and osteoblast (c_b) cell densities, connective tissue/cartilage (m_c) and bone (m_b) matrix densities, and chondrogenic (g_c) and osteogenic (g_b) growth factor concentrations in time (t) and 2D space (x, y). The model is a two-dimensional simplification of the actual three-dimensional process and accounts for many of the important events in fracture healing including haptokinetic and haptotactic mesenchymal cell migration depending on the matrix densities, space-limited cell proliferation as well as environment-dependent cell differentiation, growth factor and matrix production and degradation (Fig. 2). The model equations are given by

$$\begin{aligned}
\frac{\partial c_m}{\partial t} &= \nabla \cdot [d(m_c, m_b) \nabla c_m - v(m_c, m_b, \nabla m_c, \nabla m_b) c_m] + r_1(c_m, m_c, m_b, g_c, g_b) \\
\frac{\partial c_c}{\partial t} &= r_2(c_m, c_c, m_c, m_b, g_c, g_b) \\
\frac{\partial c_b}{\partial t} &= r_3(c_m, c_c, c_b, m_c, m_b, g_b) \\
\frac{\partial m_c}{\partial t} &= r_4(c_m, c_c, c_b, m_c) \\
\frac{\partial m_b}{\partial t} &= r_5(c_b, m_b) \\
\frac{\partial g_c}{\partial t} &= \nabla \cdot [D_{g_c} \nabla g_c] + r_6(c_c, m_c, m_b, g_c) \\
\frac{\partial g_b}{\partial t} &= \nabla \cdot [D_{g_b} \nabla g_b] + r_7(c_b, g_b)
\end{aligned} \tag{1}$$

The actual form of the functions describing the diffusion coefficient $d(m_c, m_b)$, the taxis rate $v(m_c, m_b, \nabla m_c, \nabla m_b)$ and the reactions $r_i(\dots)$ can be found in Bailón-Plaza and van der Meulen [2001]. The above equations show the general structure of the model equations and the interdependence of the seven quantities described by the model. In particular, the special form of the equation for c_m , which includes a taxis term driven by the matrix densities, is evident.

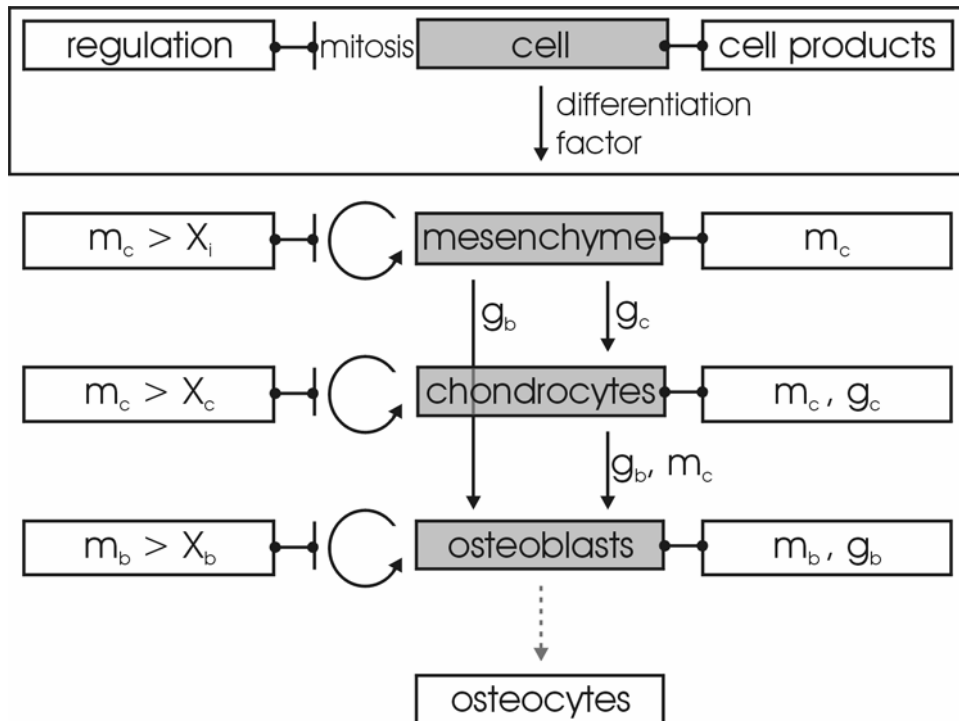


Fig. 2: Schematic representation of the mathematical model of Bailón-Plaza and van der Meulen [2001].

The set of parameter values is adapted from Bailón-Plaza and van der Meulen [2001]. The temporal parameters are scaled according to [Bailón-Plaza and van der Meulen 2003] to account for the difference in time scale of the differentiation process in rat (for which the model has been developed) and rabbit. The value of the initial concentration of mesenchymal cells, the chondrocyte proliferation and replacement rate and the cartilage degradation rate are adjusted to represent the situation in the bone chamber more accurately. The spatial domain, as depicted in Fig. 1 (lower right), represents a cut through the bone chamber. A time-limited inflow of mesenchymal cells and growth factors, via prescribed concentration values, through the chamber perforation in the outer wall and the bottom (number 2 in Fig. 1) is assumed. The bottom boundary of the domain is a symmetry line and there and on all remaining boundary parts no flow conditions apply. Initially a low fibrous tissue matrix concentration is assumed in the domain and all remaining quantities are assumed to be zero.

2.2 Simulation approach

The seven concentrations appearing in the mathematical model (1) are non-negative by nature. This qualitative property of the solution should be inherited by numerical approximations of the concentrations and hence must be obeyed by the algorithms employed in their computation. This is one essential aspect of a reliable numerical simulation. Many standard numerical techniques fail in this respect and therefore special attention is required. Furthermore, the PDE system (1) is derived based on the principle of mass conservation and this should be respected by the numerical algorithms as well. Finite volume techniques, as they are employed in this approach, are designed to automatically ensure this property. Besides those qualitative properties, other important aspects are efficiency and sufficient accuracy of the numerical scheme. The simulation technique described below meets all these requirements.

Reliable numerical methods for TDR models have been investigated extensively in Gerisch [2001], see also [Gerisch and Chaplain 2004]. The techniques developed there are adapted to the specific system at hand here. This involves a generalisation to the more complex (non-rectangle) geometry of the bone chamber. The general approach taken is the method of lines (MOL) which consists of three substeps.

(A) *Selection of a spatial grid.* The spatial domain is covered by a block-structured, rectangular grid. With each grid cell a time-dependent (spatial) average concentration value for each of the seven solution quantities is associated. The aim of the following two steps is the computation of the temporal evolution of these average concentrations.

(B) *Spatial discretisation, i.e.* approximation of the spatial derivatives of the PDE system in all grid cells by using the average concentration values in neighbouring grid cells (finite volumes approach). This leads to the so called

MOL-ODE, that is a system of coupled ordinary differential equations (ODEs) describing the temporal evolution of the average concentrations in the grid cells. The dimension of this system is the number of grid cells times the number of equations in the PDE system. In order to obtain a sufficient accuracy in the spatial discretisation a suitably fine grid is required, leading, in our case, to a MOL-ODE of dimension about 300000. One important characteristic of the selected spatial discretisation is the requirement that the resulting ODE admits only nonnegative solutions whenever the initial data is nonnegative. This is in agreement with one of the algorithmic objectives formulated above. The requirement leads to conditions on the discretisations employed for taxis, diffusion, and reaction terms. These are easily met for the reaction terms (pointwise evaluation) and the discretisation of the diffusion term (standard second-order central differences). However, the discretisation of the taxis term is not straightforward under these conditions and upwinding techniques with nonlinear limiter functions (van Leer limiter) are employed in order to satisfy them. Section 2.3 demonstrates by means of an example the necessity of such a special taxis discretisation. A more detailed discussion of the spatial discretisation can be found in Gerisch [2001].

(C) *Time integration of the MOL-ODE, i.e.* approximations to the solution of the MOL-ODE, as obtained in substep (B), are computed at discrete time points. Due to the enormous size of the MOL-ODE this requires very efficient numerical techniques. As a rule, ODE systems arising from the discretisation of PDEs involving diffusion terms are referred to as *stiff* systems and call for implicit time integration schemes. Furthermore, the method employed should have an automatic time step size control, which ensures that the error caused in each time step (local error) is below a user-prescribed tolerance while at the same time using as little computational effort (time) as possible. Such a method is implemented in the efficient and reliable code ROWMAP [Weiner *et al.* 1997] which is used for the simulations described here.

The numerical scheme described above has been implemented in a simulation tool in the FORTRAN programming language. This tool allows the user to run simulations interactively as well as automatically and to adapt the model parameters, model equations and boundary conditions in a straightforward way.

2.3 Illustration of the special taxis discretisation

In order to illustrate point (B) above more clearly and to give a motivation for the special taxis discretisation employed, a gross simplification of the equation for c_m of the model (which contains the taxis term) is considered here. Restrictions are made to one spatial dimension (x), diffusion and reaction are neglected completely, and the taxis function $v(m_c, m_b, \nabla m_c, \nabla m_b)$ is replaced by a positive constant a . This results in the linear advection equation

$$\frac{\partial u(t, x)}{\partial t} + a \cdot \frac{\partial u(t, x)}{\partial x} = 0$$

with constant velocity a . Given an initial profile $u_0(x)$ at time zero, the exact solution is given by $u(t, x) = u_0(x - at)$, that is the initial profile is advected unchanged to the right with velocity a . Now the numerical solution of this problem is investigated. Consider N grid cells (finite volumes) of equal length h covering the spatial domain and denote the i th cell by $V_i = [x_i - h, x_i]$. Let $u_i(t)$ be the average of $u(t, x)$ on V_i . The temporal evolution of $u_i(t)$ is then exactly described by the equation

$$u_i'(t) = - \frac{[a \cdot u(t, x_i) - a \cdot u(t, x_i - h)]}{h}. \quad (2)$$

Here $a \cdot u(t, x_i)$ is the flux (or flow of material) through x_i at time t . The aim is to compute approximations $U_i(t)$ of the exact cell averages $u_i(t)$. To this end we must find a computable estimate $F(t, x_i)$ of the flux $a \cdot u(t, x_i)$ on the cell interfaces. This is achieved by letting the numerical flux $F(t, x_i)$ depend on the (computable) approximations $\dots, U_{i-1}(t), U_i(t), U_{i+1}(t), \dots$ of the exact cell averages in neighbouring grid cells only. This allows to replace the exact equation (2) by the approximation

$$U_i'(t) = - \frac{[F(t, x_i) - F(t, x_i - h)]}{h}.$$

Using this approach for each of the N grid cells (with some special treatment near the boundary of the domain) the MOL-ODE system of dimension N is obtained. This completes substep (B) of the method of lines. In the following we discuss the choice of the numerical flux $F(t, x_i)$.

One simple choice for the numerical flux is motivated by the underlying physics of the flow: the flow comes from the left (upstream) and therefore the flux can be approximated by $F(t, x_i) = a \cdot U_i(t)$. This results in the ODE

$$U_i'(t) = - \frac{a[U_i(t) - U_{i-1}(t)]}{h}.$$

The resulting scheme is a first-order accurate approximation of the linear advection equation and called the first-order upwind method. Applying this method to a nonnegative initial profile $u_0(x)$ leads to a nonnegative numerical solution without oscillations, but one recognizes a considerable smearing out of the profile, see Fig. 3 (left column). This diffusive character of the scheme, which can be analysed rigorously, can be reduced by decreasing the interval length h and hence, at the same time, increasing the dimension N of the MOL-ODE system. However, an extremely fine grid is required in order to resolve steep gradients accurately and this is in general prohibitively expensive in terms of computing time for the subsequent solution of the MOL-ODE, *i.e.* substep (C). Therefore it is more advisable to seek a more accurate approximation of the advection equation. This can be achieved by approximating the fluxes on cell interfaces with $F(t, x_i) = a \cdot (U_{i+1}(t) + U_i(t)) / 2$, *i.e.* by using the averages on both sides of the cell interface at x_i . This leads to

$$U_i'(t) = - \frac{a[U_{i+1}(t) - U_{i-1}(t)]}{2h},$$

which is known as the second-order central approximation of the linear advection equation. Applying this scheme to a smooth nonnegative initial profile results in a much improved numerical solution compared to the first-order scheme, see Fig. 3 (upper row, middle plot). However, if the initial profile contains steep fronts – as they are often present in models from evolutionary biology including the one considered in this work – then the weaknesses of the central scheme become apparent: although no diffusive character of the scheme is present, a dispersive character can be observed that leads to unphysical oscillations in the solution and subsequently negative concentration values, see Fig. 3 (lower row, middle plot). This is clearly unacceptable because if reactions are present in the model then negative (concentration) values might render them unstable. Setting negative solution values to zero is no general option either since this interferes with the mass balances and hence can have a critical influence on steady states of the system.

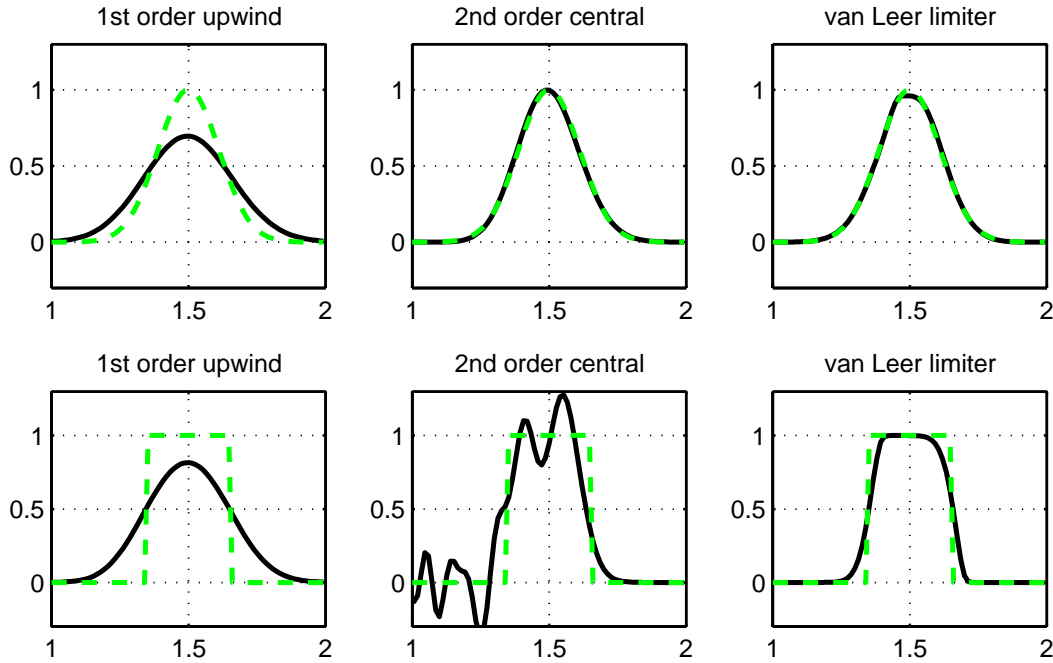


Fig. 3: Solutions of the linear advection equation with velocity $a = 1$ at time $t = 1$. The dashed lines are exact solutions and the solid lines are numerical approximations. The length of each grid cell in the numerical scheme is $h = 1 / 75$. The initial profile is a smooth wave (upper row) or a block (lower row). The discretisation of the advective term is first-order upwind (left column), second-order central (middle column), and limited with van Leer limiter (right column).

A combination of the properties of both approaches is what seems to be desirable: high accuracy in smooth regions of the solution and no negative solution values or oscillations anywhere. This can be achieved. To this end a flux approximation is considered of the form

$$F(t, x_i) = a \left(U_i(t) + \frac{1}{2} L(r_i) (U_i(t) - U_{i-1}(t)) \right),$$

with a smoothness monitor function r_i of the solution defined by

$$r_i = \frac{U_{i+1}(t) - U_i(t)}{U_i(t) - U_{i-1}(t)}$$

and a so-called limiter function $L(r)$. Note that r_i is negative at local maxima or minima of the solution and about one in smooth regions. Observe further that for $L(r_i) = 0$ the first-order upwind flux is recovered whereas for $L(r_i) = r_i$ the second-order central flux is obtained. From the discussion above it is clear that $L(r_i)$ should be about one in smooth regions of the solution but close to or even zero in regions where a higher-order discretisation leads to negative solution values or oscillations. So the task of the limiter function is to smoothly switch between a first-order and a higher-order scheme depending on the local behaviour of the problems solution. This can be achieved, for instance, by choosing the van Leer limiter function

$$L(r) = \frac{r + |r|}{1 + |r|} .$$

The result of this approach can be seen in Fig. 3 (right column). A nonnegative solution without oscillations is obtained and the solution is smeared out only locally around local maxima or minima where the limiter selects the diffusive first-order upwind discretisation. Hence there is a good qualitative and quantitative agreement of the numerical solution and the exact solution.

The approach described above can be generalised to the full TDR system (1) describing tissue differentiation in the bone chamber and was used for the simulations reported in Section 3. Details can be found in [Gerisch 2001]. The excellent textbook by Hundsdorfer and Verwer [2003] discusses many more computational aspects, also in the context of biomedical applications.

3 Results, discussion and future research

Examples of the solution output are shown in Fig. 4. The upper part of the figure shows three snapshot sequences of the mesenchymal cell density (upper), concentration of the fibrous tissue/cartilage extracellular matrix (ECM, middle) and concentration of bone ECM (lower). A wave of mesenchymal cells travels through the chamber in eight days. In the presence of the chondrogenic growth factor, these precursor cells differentiate into chondrocytes. When the cell density c_c is sufficiently high, the chondrocytes start depositing the cartilage matrix, filling the entire chamber with high density cartilage by day 30. When the cartilage density has reached a critical value (representing the chondrocytes maturation) the endochondral replacement process under the influence of the osteogenic growth factor will start. At day 60 the chamber is filled with a bony ECM. This endpoint result is in qualitative agreement with the experimental observations showing a lot of bone in the chamber after 12 weeks (84 days). The lower part of Fig. 4 shows the evolution of the percentage of the chamber filled with fibrous tissue/cartilage ECM (left) and bone ECM (right). It clearly shows

the process of endochondral replacement starting from a chamber filled with cartilage around day 40 and ending around day 60 with a chamber entirely filled with a bone ECM.

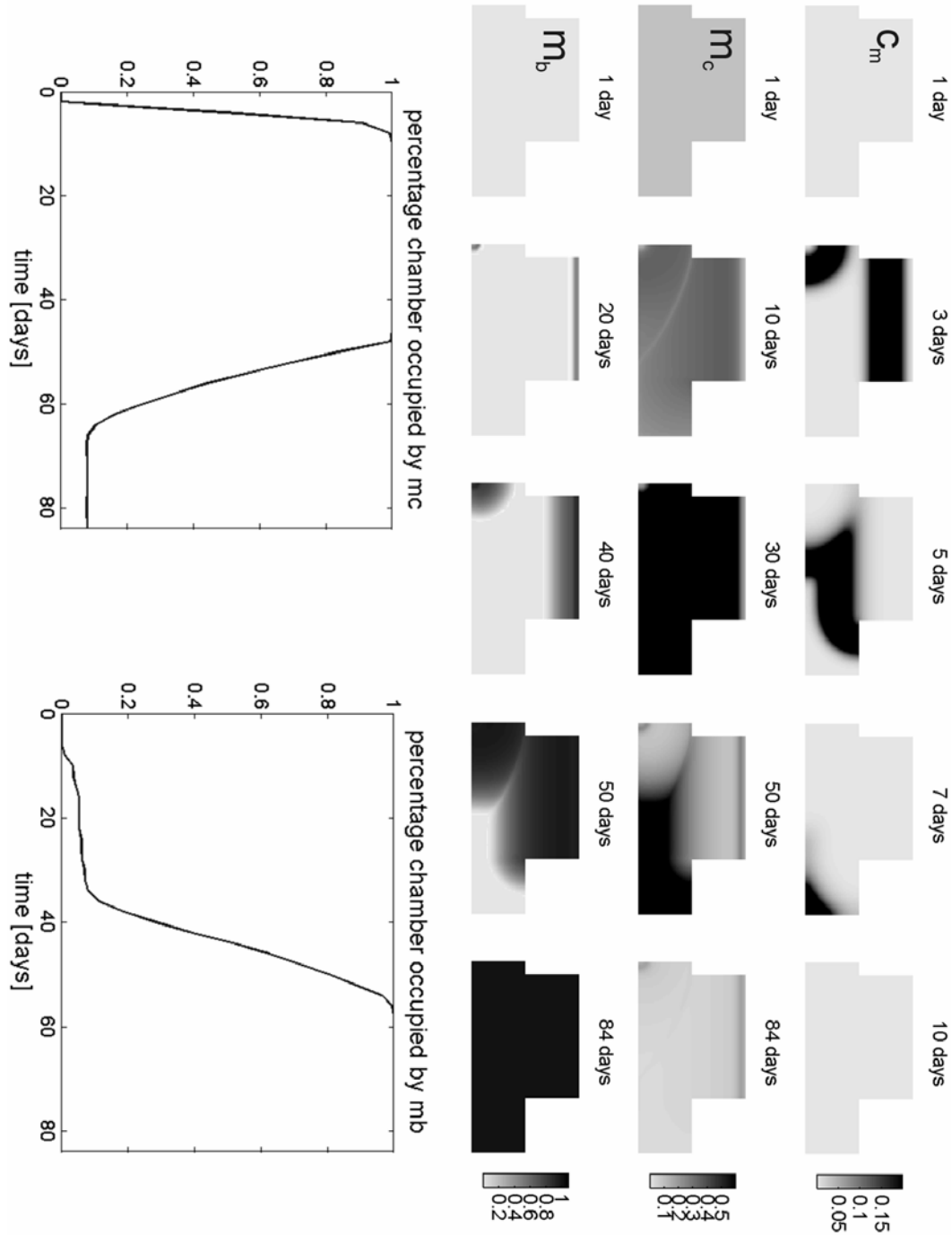


Fig. 4: Upper: simulation snapshots of the wave of mesenchymal cell density (c_m), the density of fibrous tissue/cartilage ECM (m_c) and bone ECM (m_b). Lower: percentage of the chamber occupied by fibrous tissue/cartilage ECM (m_c - left) and bone ECM (m_b - right).

A simulation of the tissue differentiation model for 12 weeks with the algorithm described takes about 40 minutes computation time on a standard PC with Intel Pentium 4 processor. This is very efficient taking into account that the dimension of the MOL-ODE is about 300000. The solutions returned by the algorithm are nonnegative up to an error of the order of a user-prescribed tolerance at most, and hence also this objective has been achieved clearly.

The endpoint result of the numerical simulation is in qualitative agreement with experimental observations. However, quantitatively we expect a further improvement by carefully adjusting model parameters and boundary conditions in the future. Another area of future research is to couple the biological model investigated here with a structural mechanics model in order to additionally account for mechanical effects in tissue differentiation during bone growth, fracture healing and implant osseointegration.

References

Bailón-Plaza, A., van der Meulen, M.C.H., A mathematical framework to study the effects of growth factor influences on fracture healing, *Journal of Theoretical Biology*, 2001, 212, 191–209.

Bailón-Plaza, A., van der Meulen, M.C.H., Beneficial effects of moderate, early loading and adverse effects of delayed or excessive loading on bone healing, *Journal of Biomechanics*, 2003, 36, 1069–1077.

Bertram, J.E.A., Swartz, M.S., The law of bone transformation: a case of Crying Wolff? *Biology Reviews*, 1991, 66, 245–273.

Carter, D.R., Mechanical loading histories and cortical bone remodeling. *Calcified Tissue International*, 1984, 36 (Suppl. 1), S19–24.

Claes, L.E., Heigele, C.A., Magnitudes of local stress and strain along bony surfaces predict the course and type of fracture healing, *Journal Biomechanics*, 1999, 32(3), 255–266.

Duyck, J., De Cooman, M., Puers, R., Van Oosterwyck, H., Vander Sloten, J., Naert, I., A repeated sampling bone chamber methodology for the evaluation of tissue differentiation and bone adaptation around titanium implants under controlled mechanical conditions, *Journal of Biomechanics*, 2004, In press.

Geris, L., Andreykiv, A., Van Oosterwyck, H., Vander Sloten, J., van Keulen, F., Duyck, J., Naert, I., Numerical simulation of tissue differentiation around loaded titanium implants in a bone chamber, *Journal of Biomechanics*, 2004, 37, 763–769.

Gerisch, A., Numerical Methods for the Simulation of Taxis-Diffusion-Reaction Systems, PhD thesis, Martin-Luther-Universität Halle-Wittenberg, 2001.

Gerisch, A., Chaplain, M.A.J., Robust Numerical Methods for Taxis-Diffusion-Reaction Systems: Application to Biomedical Problems, *Mathematical and Computer Modelling*, 2004, In press.

Hundsdoerfer, W., Verwer, J.G., Numerical Solution of Time-Dependent Advection-Diffusion-Reaction Equations, No. 33 in Springer Series in Computational Mathematics, Springer-Verlag Berlin Heidelberg, 2003.

Koo, L.Y., Irvine, D.J., Mayes, A.M., Lauffenburger, D.A., Griffith, L.G., Co-regulation of cell adhesion by nanoscale RGD organization and mechanical stimulus, *Journal of Cell Science*, 2002, 115, 1423–1433.

Prendergast, P.J., Huiskes, R. and Søballe, K., Biophysical stimuli on cells during tissue differentiation at implant interfaces, *Journal of Biomechanics*, 1997, 30(6), 539–548.

Vortkamp, A., Pathi, S., Peretti, G.M., Caruso, E.M., Zaleske, D.J., Tabin, C.J., Recapitulation of signals regulating embryonic bone formation during postnatal growth and in fracture repair, *Mechanisms of Development*, 1998, 71, 65–76.

Weiner, R., Schmitt, B.A., Podhaisky, H., ROWMAP — a ROW-code with Krylov techniques for large stiff ODEs, *Appl. Numer. Math.*, 1997, 25, 303–319.

You, L., Cowin, S.C., Schaffler, M.B., Weinbaum, S., A model for strain amplification in the actin cytoskeleton of osteocytes due to fluid drag on pericellular matrix, *Journal of Biomechanics*, 2001, 34, 1375–1386.